doi:10.1038/nature18322

The first gravitational-wave source from the isolated evolution of two stars in the 40–100 solar mass range

Krzysztof Belczynski[1], Daniel E. Holz[2], Tomasz Bulik[1] & Richard O'Shaughnessy[3]

The merger of two massive (about 30 solar masses) black holes has been detected in gravitational waves[1]. This discovery validates recent predictions[2–4] that massive binary black holes would constitute the first detection. Previous calculations, however, have not sampled the relevant binary-black-hole progenitors—massive, low-metallicity binary stars—with sufficient accuracy nor included sufficiently realistic physics to enable robust predictions to better than several orders of magnitude[5–10]. Here we report high-precision numerical simulations of the formation of binary black holes via the evolution of isolated binary stars, providing a framework within which to interpret the first gravitational-wave source, GW150914, and to predict the properties of subsequent binary-black-hole gravitational-wave events. Our models imply that these events form in an environment in which the metallicity is less than ten per cent of solar metallicity, and involve stars with initial masses of 40–100 solar masses that interact through mass transfer and a common-envelope phase. These progenitor stars probably formed either about 2 billion years or, with a smaller probability, 11 billion years after the Big Bang. Most binary black holes form without supernova explosions, and their spins are nearly unchanged since birth, but do not have to be parallel. The classical field formation of binary black holes we propose, with low natal kicks (the velocity of the black hole at birth) and restricted common-envelope evolution, produces approximately 40 times more binary-black-holes mergers than do dynamical formation channels involving globular clusters[11]; our predicted detection rate of these mergers is comparable to that from homogeneous evolution channels[12–15]. Our calculations predict detections of about 1,000 black-hole mergers per year with total masses of 20–80 solar masses once second-generation ground-based gravitational-wave observatories reach full sensitivity.

We study the formation of coalescing black-hole binaries using the StarTrack population synthesis code[16,17]. This method has been updated to account for the formation of massive black-hole systems in isolated stellar environments. The new key factors include an observationally supported star-formation rate, chemical enrichment across cosmic time and a revised initial condition for evolution of binary stars. Hitherto, simulations have been unable to achieve the desired predictive power because of the limitations on the input physics (for example, limited metallicity range) and numerical accuracy. To ensure the dominant contribution from intrinsically rare low-metallicity star-forming environments are adequately sampled, we use a dense grid of metallicities (32 metallicities) with high precision (20 million binaries each).

Although binary population synthesis is dependent on a number of uncertain physical factors, there has been recent progress in reducing this uncertainty and understanding how it affects predictions. In light of this, we consider the following three models to encompass major sources of uncertainty (Methods): M1 represents our 'standard' classical formation model for double compact objects composed of two black holes (BH–BH), two neutron stars (NS–NS), or one of each (BH–NS); M2 is our 'optimistic' model, in which Hertzsprung-gap stars may initiate and survive common-envelope evolution, leading to many more binaries being formed; and M3 is our 'pessimistic' model, in which black holes receive large natal kicks, which disrupts and thereby reduces the number of BH–BH progenitor binaries.

For each generated double compact object merger, with its intrinsic component masses and the redshift of the merger, we estimate the probability that such a merger would have been detectable in the first observing run (O1) of the Laser Interferometer Gravitational-Wave Observatory (LIGO) advanced detectors. We adopt a self-consistent model of evolution of stellar populations in the Universe[3,4], and we take the representative noise curve for O1 (https://dcc.ligo.org/LIGO-G1501223/public) and assume 16 days of coincident science-quality observational time[1].

In Fig. 1 we show the formation and evolution of a typical binary system that result in a merger with similar masses and at a similar time to GW150914. Stars that form such mergers are very massive ($40M_\odot$–$100M_\odot$; $M_\odot$ is the mass of the Sun), and at the end of their lives they collapse directly to form black holes[18]. Because there is no associated supernova explosion, there is also no mass ejection. We allow 10% of the collapsing stellar mass to be emitted in neutrinos. If natal kicks are associated with asymmetric mass ejection (as in our standard model), then our prediction is that these massive black holes do not receive natal kicks and that their spin directions are the same as that of their progenitor collapsing stars. The binary evolution removes the hydrogen-rich envelope from both binary components, making both stars compact and luminous Wolf–Rayet stars before they collapse to black holes. The first binary interaction is a dynamically stable Roche-lobe overflow phase, whereas the second interaction consists of a common-envelope phase that produces a compact binary. After the common-envelope phase, the progenitor binary resembles two known high-mass X-ray binaries hosting massive black holes: IC10 X-1 and NGC 300 X-1 (ref. 19). A massive BH–BH binary (each with a mass of approximately $30M_\odot$) is formed in approximately 5 Myr of evolution, with a relatively wide orbit (semi-major axis $a \approx 50R_\odot$; $R_\odot$ is the radius of the Sun), leading to a long time to coalescence of $t_{\mathrm{merger}} \approx 10$ Gyr. The accretion onto the first black hole in the common-envelope phase is only modest (approximately $1.5M_\odot$), whereas accretion from stellar wind of its companion is rather small (less than $0.1M_\odot$).

To investigate general aspects of the formation history of GW150914, we select a population of GW150914-like BH–BH mergers with a total redshifted mass of $M_{\mathrm{tot},z} = 54M_\odot$–$73M_\odot$, and then further restrict our sample to binaries that would be detectable in O1. The formation channels typical for these massive BH–BH mergers are summarized in Extended Data Table 1.

We find that the most likely progenitor of GW150914 consists of a primary star in the mass range $40M_\odot$–$100M_\odot$ and a secondary in the mass range $40M_\odot$–$80M_\odot$. In our standard model, the binary formed

[1]Astronomical Observatory, Warsaw University, Ujazdowskie 4, 00-478 Warsaw, Poland. [2]Enrico Fermi Institute, Department of Physics, Department of Astronomy and Astrophysics, and Kavli Institute for Cosmological Physics, University of Chicago, Chicago, Illinois 60637, USA. [3]Center for Computational Relativity and Gravitation, Rochester Institute of Technology, Rochester, New York 14623, USA.

© 2016 Macmillan Publishers Limited. All rights reserved

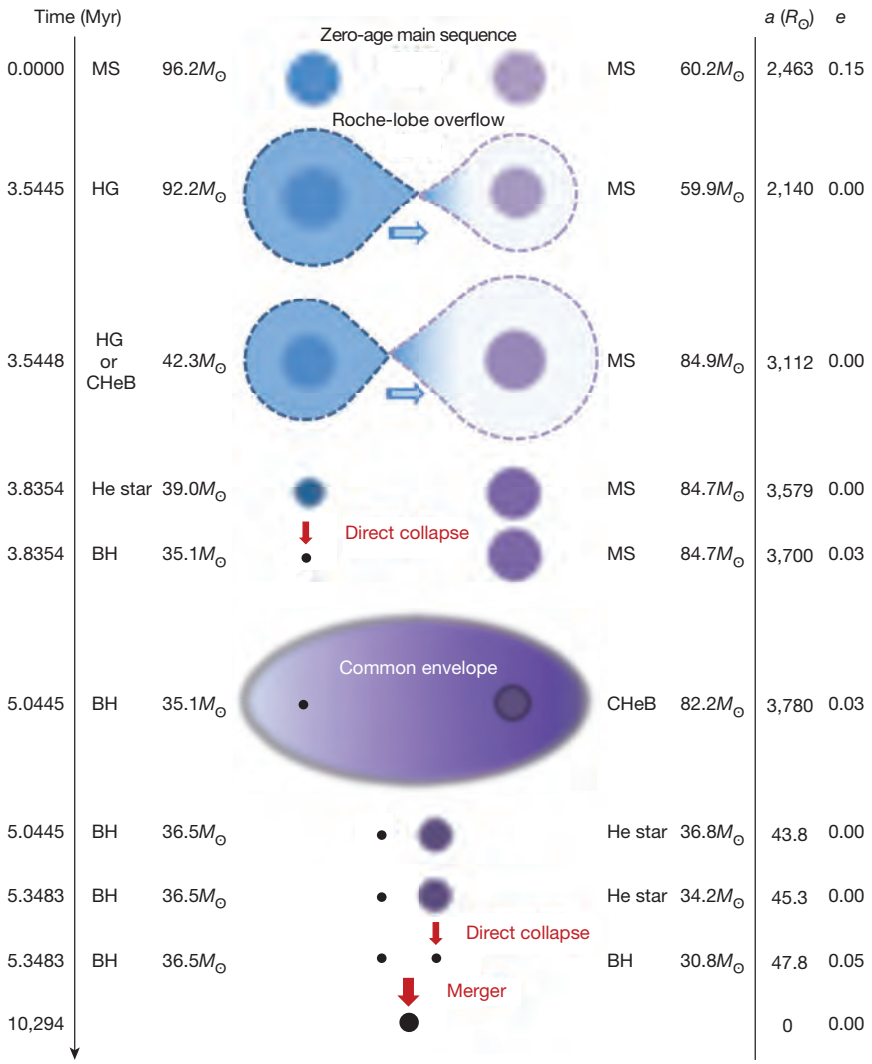

Figure 1 | Example binary evolution leading to a BH–BH merger similar to GW150914. A massive binary star ($96M_\odot$ (blue) + $60M_\odot$ (purple)) is formed in the distant past (2 billion years after Big Bang; $z \approx 3.2$; top row), and after 5 million years of evolution forms a BH–BH system ($37M_\odot + 31M_\odot$; second-last row). For the ensuing 10.3 billion years, this BH–BH system is subject to loss of angular momentum, with the orbital separation steadily decreasing, until the black holes coalesce at redshift $z = 0.09$. This example binary formed in a low-metallicity environment ($Z = 0.03Z_\odot$). MS, main-sequence star; HG, Hertzsprung-gap star; CHeB, core-helium-burning star; BH, black hole; a, orbital semi-major axis; e, eccentricity.

in a low-metallicity environment ($Z < 0.1Z_\odot$; $Z_\odot$ is the metallicity of the Sun; see Extended Data Fig. 1) and either in the early Universe (2 Gyr after the Big Bang) or very recently (11 Gyr after the Big Bang).

The distribution of birth times of these massive BH–BH mergers is bimodal (Fig. 2 and Extended Data Fig. 2), with a majority of systems originating from the distant past (55% of binaries; about 2 Gyr after the Big Bang, corresponding to $z \approx 3$) and a smaller contribution from relatively young binaries (25%; formed about 11 Gyr after the Big Bang, corresponding to $z \approx 0.2$). This bimodality arises from two naturally competing effects: on the one hand, most low-metallicity star formation occurs in the early Universe; on the other hand, in contrast to previous work[3,4], significantly more low-metallicity star formation is currently expected to occur in the low-redshift Universe[20]. Therefore, as is the case with binary neutron stars, we anticipate a significant contribution to the present-day binary-black-hole merger rate from binary black holes formed in low-redshift, low-metallicity star-forming regions. The delay-time distribution of BH–BH binaries in our simulations follows a $1/t$ distribution. The birth times therefore naturally pile up at low redshifts ($z \approx 0.1$–0.3) and this gives rise to a low-z peak (Extended Data Fig. 2a). However, the low-metallicity ($Z < 0.1Z_\odot$) star formation responsible for the production of massive BH–BH mergers peaks at a redshift of $z \approx 3$ (Extended Data Fig. 2b). The convolution of these two effects produces the bimodal birth-time distribution (Extended Data Fig. 2c).

These massive GW150914-like mergers consist of black holes with comparable masses. The vast majority (99.8%) of mergers are found with mass ratios in the range $q = 0.7$–1.0 (Extended Data Fig. 3), with the mass ratio of GW150914 ($q = 0.82^{+0.16}_{-0.21}$) falling near the centre of the expected region. The formation of low-mass-ratio objects is suppressed because low-mass-ratio progenitors tend to merge during the first mass-transfer event when the more massive component overfills its Roche lobe[21]. However, with decreasing total merger mass, the mass ratio extends to lower values. In particular, for the lower mass bin of $M_{\mathrm{tot},z} = 25M_\odot$–$37M_\odot$, mass ratios as low as $q = 0.3$ are also found.

We now use our full sample of double compact object mergers to make predictions for the merger-rate density, detection rates and merger mass distribution. The results are shown in Fig. 3 and Extended Data Table 1, in which we compare them to the measured values inferred from O1 LIGO observations. We find an overall detection rate that is consistent with the detection of one significant candidate (GW150914) during the principal 16-day double coincident period (when both LIGO gravitational-wave interferometers are operating simultaneously) for our standard model (M1), but that is inconsistent for our other two models (optimistic M2 and pessimistic M3; more detail below).

The BH–BH merger rates inferred from the 16 days of O1 LIGO observations are in the range 2–400 $\mathrm{Gpc^{-3}\,yr^{-1}}$ (ref. 22). For comparison, we estimate the rate density of binary black holes from our population synthesis dataset. We consider the full population of binary black holes within a redshift of $z = 0.1$ (that is, not weighted by their detection probability) and calculate their average source-frame merger-rate density. We find a value of 218 $\mathrm{Gpc^{-3}\,yr^{-1}}$ for our standard model (M1), which is in good agreement with the inferred LIGO rate[22]. By contrast, our optimistic model (M2) predicts too many mergers, with a rate density of 1,303 $\mathrm{Gpc^{-3}\,yr^{-1}}$, and our pessimistic model (M3)

© 2016 Macmillan Publishers Limited. All rights reserved

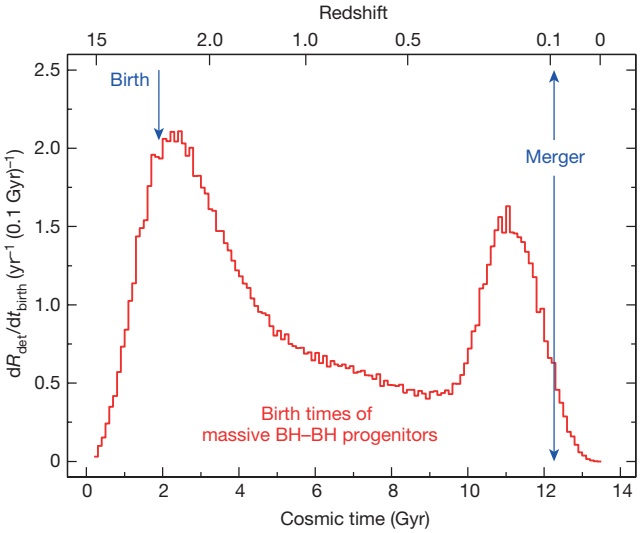

Figure 2 | Birth times of GW150914-like progenitors across cosmic time. dR_{det}/dt represents the contribution to the detection rate from binaries in a given 0.1-Gyr bin of birth time. Half of the binaries that form BH–BH mergers detectable in O1 with total redshifted mass in the range $M_{tot,z}=54M_{\odot}$–$73M_{\odot}$ were born within 4.7 Gyr of the Big Bang (corresponding to $z>1.2$). The birth and merger times of the binary depicted in Fig. 1 are marked in blue; this binary follows the most typical evolutionary channel for massive BH–BH mergers (BHBH1 in Extended Data Table 1). The merger redshift of GW150914 is $z=0.088$. The bimodal shape of the distribution originates from a combination of the BH–BH delay-time distribution and the low-metallicity star-formation history (see Extended Data Fig. 2 for details).

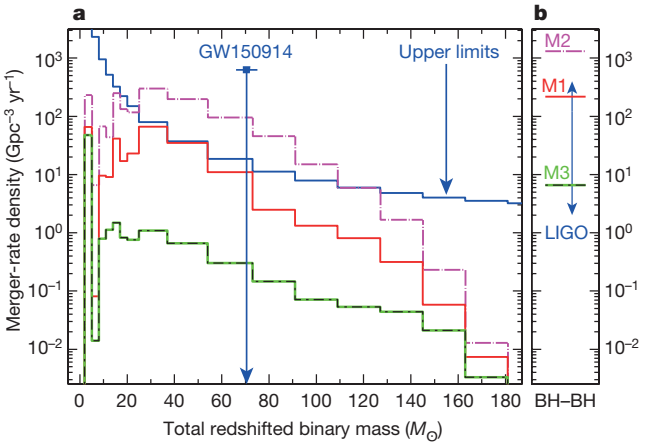

Figure 3 | Comparison of merger rates and masses with O1 LIGO results. Results are shown for standard (M1; red solid lines), optimistic common-envelope phase (M2; pink dash-dotted lines) and pessimistic large black-hole kicks (M3; green/black solid/dash-dotted line) models. **a**, Distribution of total redshifted binary mass. The merger-rate density of GW150914 ($70.5M_{\odot}$) is indicated by the blue square (with 90% confidence interval in mass, and its vertical position arbitrary). The blue solid line shows the fiducial estimate of the sensitivity (or upper limits) of the 16-day O1 run. A comparison of the shapes of the blue and red lines suggests that the most likely detections for M1 are BH–BH mergers with masses in the range $25M_{\odot}$–$73M_{\odot}$. NS–NS mergers (first bin) and BH–NS mergers (next five bins) are well below the estimated sensitivity and thus detections in O1 are not expected. The rate densities are in the detector rest frame. **b**, Comparison of the LIGO estimate of the BH–BH merger rate with our models. The LIGO value of 2–400 Gpc^{-3} yr^{-1} (90% credible range) compares well with our standard (M1) and large black-hole natal kicks (M3) models. The rate densities are in the source rest frame. An updated version of Fig. 3, including additional gravitational-wave detections as they occur, can be found at http://www.syntheticuniverse.org/stvsgwo.html.

is at the very bottom end of the allowable range with a predicted rate of 6.6 Gpc^{-3} yr^{-1}. In our models, the BH–BH merger-rate density increases with redshift (Extended Data Fig. 4). This increase is modest; our predicted source-frame BH–BH merger-rate density would double if the cut-off redshift was increased from $z=0.1$ to $z=0.6$.

The merger-rate density for the model with an optimistic common-envelope phase (M2) is an order of magnitude larger than the rate estimate from LIGO. This implies that unevolved massive stars (during main sequence and Hertzsprung gap) do not initiate/survive the common-envelope phase[9,23]. In our classical BH–BH formation scheme, only evolved stars (during core helium burning) with well-developed convective envelopes are allowed to initiate and survive the common-envelope phase.

Our predictions for the pessimistic model (M3) imply that large natal kicks (with average magnitudes of more than about 400 km s^{-1}) are unlikely for massive black holes. This model predicts that an event such as GW150914 would happen only 1% of the time, with the detection of any BH–BH system happening less than 10% of the time (Table 1). In principle, this conclusion applies to the formation of only the first black hole in the binary, because large natal kicks lead to disruption of BH–BH progenitors while the binaries are wide. During the formation of the second black hole, the progenitor binaries are on very close orbits (Fig. 1) and are not disrupted by natal kicks. In Extended Data Fig. 4 we show a sequence of models with intermediate black-hole natal kicks; future observations may allow us to discriminate between these models and to constrain the natal-kick distribution. Future observations converging on M1 would indicate no natal kicks nor supernova explosions in massive black-hole formation[18]. A striking ramification of this is the prediction that hot and luminous Wolf–Rayet progenitors of massive black holes[24] should disappear from the sky as a result of direct collapse to a black hole (that is, with no supernova explosion). Targeted observational campaigns to search for such phenomena are already underway[25].

Figure 3 shows the relative contribution to the overall merger-rate density associated with each bin of total redshifted merger mass $M_{tot,z}$. For comparison, Fig. 3 also shows the fiducial sensitivity (see Methods) as a function of mass, assuming equal-mass zero-spin binary black holes. Figure 3 demonstrates that the intersection of the strongly mass-dependent sensitivity and the intrinsic detectable mass distribution strongly favours sources with total redshifted masses of $25M_{\odot}$–$73M_{\odot}$, consistent with recent work[4] and total redshifted mass of GW150914 ($M_{tot,z}=70.5M_{\odot}$). In our simulations, the maximum intrinsic mass of a merging BH–BH binary is $M_{tot}=140M_{\odot}$. When accounting for cosmological redshift

Table 1 | Expected detection rate and number of detections

Model	Merger type	O1 detection rate (yr^{-1})	Number of detections in 16 days of O1
M1	All	63.18	2.770
	NS–NS	0.052	0.002
	BH–NS	0.231	0.010
	BH–BH	62.90	2.758
	GW150914	11.95	0.524
M2	All	476.1	20.87
	NS–NS	0.191	0.008
	BH–NS	0.796	0.035
	BH–BH	475.1	20.83
	GW150914	110.0	4.823
M3	All	1.985	0.087
	NS–NS	0.039	0.002
	BH–NS	0.014	0.001
	BH–BH	1.932	0.085
	GW150914	0.270	0.012

The first column indicates the model: standard (M1), optimistic common-envelope phase (M2), and large black-hole kicks (M3). The third column lists the expected detection rate R_{det} per unit double coincident time (both LIGO detectors operating at appropriate sensitivity), for a network comparable to O1, for different classes of mergers (indicated in the second column). The fourth column shows $R_{det}T$, where $T=16$ days is the analysis time relevant for the rate estimate for GW150914 (ref. 22). Entries for merger type 'GW150914' are for the subpopulation of BH–BH mergers with total redshifted mass in the range $M_{tot,z}=54M_{\odot}$–$73M_{\odot}$.

© 2016 Macmillan Publishers Limited. All rights reserved

($M_{\mathrm{tot},z} = (1+z)M_{\mathrm{tot}}$) and taking into account the advanced O1 horizon redshift for this most massive binary ($z = 0.7$), the highest possible observed mass within O1 would be approximately $240M_{\odot}$.

Spin magnitudes and directions of merging black holes are potentially measurable by LIGO[1]. The second-born black hole in a BH–BH binary does not accrete mass, and its spin at merger is unchanged from its spin at birth. The first-born black hole, on the other hand, has a chance to accrete material from the stellar wind of the unevolved companion or during common-envelope evolution. However, because this is limited either by the very low efficiency of accretion from stellar winds or by inefficient accretion during common-envelope evolution[26,27], the total accreted mass onto the first-born black hole is expected to be rather small (about $1M_{\odot}$–$2M_{\odot}$). This is insufficient to significantly increase the spin, and thus the spin magnitude of the first-born black hole at merger is within about 10% of its birth spin.

In our modelling, we assume that stars that are born in a binary have their spins aligned with the angular-momentum vector of the binary. If massive black holes do not receive natal kicks (for example, in our standard model M1), then our prediction is that black-hole spins are aligned during the final massive BH–BH merger. We note that our standard model includes natal kicks and mass loss for low-mass black holes (less than about $10M_{\odot}$), and therefore BH–BH binaries with one or two low-mass black holes may show misalignment. Alternatively, binaries could be born with misalignment and retain it, misalignment could be caused by the third body or by interaction between the radiative envelope and the convective core[28], or misalignment could result from a large natal kick on the second-born black hole. Several binaries are reported with misaligned spins[29]. Therefore, spin alignment of massive merging black holes suggests isolated field evolution, while misaligned spins do not elucidate formation processes.

As shown in Fig. 1, we find that the formation of massive BH–BH mergers is a natural consequence of isolated binary evolution. Our standard model (M1) of BH–BH mergers fully accounts for the observed merger-rate density and merger mass (Fig. 3), and for the mass ratio of two merging black holes (Extended Data Fig. 3) inferred from GW150914.

Our standard formation mechanism (M1) produces significantly more binary black holes than do alternative, dynamical channels associated with globular clusters. A recent study[11] suggests globular clusters could produce a typical merger rate of 5 $\mathrm{Gpc^{-3}\,yr^{-1}}$; our standard model (M1) BH–BH merger-rate density is about 40 times larger: 218 $\mathrm{Gpc^{-3}\,yr^{-1}}$.

However, one non-classical isolated binary evolution channel involving rapidly rotating stars (homogeneous evolution) in very close binaries may also fully account for the formation of GW150914 (refs 12–15). In particular, typical rates of 1.8 detections in 16 days of O1 observations are found[13], which is comparable to our prediction of 2.8 (Table 1). Only very massive BH–BH mergers with total intrinsic masses of more than about $50M_{\odot}$ are formed in this model[12,13], whereas our model predicts mergers with masses in a broader range, down to greater than about $10M_{\odot}$. Future LIGO observations of BH–BH mergers may allow us to discriminate between these two very different mass distributions/models.

Online Content Methods, along with any additional Extended Data display items and Source Data, are available in the online version of the paper; references unique to these sections appear only in the online paper.

Received 21 February; accepted 11 May 2016.

1. Abbott, B. P. *et al.* Observation of gravitational waves from a binary black hole merger. *Phys. Rev. Lett.* **116,** 061102 (2016).
2. Belczynski, K. *et al.* The effect of metallicity on the detection prospects for gravitational waves. *Astrophys. J.* **715,** L138–L141 (2010).
3. Dominik, M. *et al.* Double compact objects. III. Gravitational-wave detection rates. *Astrophys. J.* **806,** 263 (2015).
4. Belczynski, K. *et al.* Compact binary merger rates: comparison with LIGO/Virgo upper limits. *Astrophys. J.* **819,** 108 (2016).
5. Tutukov, A. V. & Yungelson, L. R. The merger rate of neutron star and black hole binaries. *Mon. Not. R. Astron. Soc.* **260,** 675–678 (1993).
6. Lipunov, V. M., Postnov, K. A. & Prokhorov, M. E. Black holes and gravitational waves: possibilities for simultaneous detection using first-generation laser interferometers. *Astron. Lett.* **23,** 492–497 (1997).
7. Nelemans, G., Yungelson, L. R. & Portegies Zwart, S. F. The gravitational wave signal from the Galactic disk population of binaries containing two compact objects. *Astron. Astrophys.* **375,** 890–898 (2001).
8. Voss, R. & Tauris, T. M. Galactic distribution of merging neutron stars and black holes – prospects for short gamma-ray burst progenitors and LIGO/VIRGO. *Mon. Not. R. Astron. Soc.* **342,** 1169–1184 (2003).
9. Belczynski, K., Taam, R. E., Kalogera, V., Rasio, F. A. & Bulik, T. On the rarity of double black hole binaries: consequences for gravitational wave detection. *Astrophys. J.* **662,** 504–511 (2007).
10. Mennekens, N. & Vanbeveren, D. Massive double compact object mergers: gravitational wave sources and r-process element production sites. *Astron. Astrophys.* **564,** A134 (2014).
11. Rodriguez, C. L., Chatterjee, S. & Rasio, F. A. Binary black hole mergers from globular clusters: masses, merger rates, and the impact of stellar evolution. *Phys. Rev. D* **93,** 084029 (2016).
12. Marchant, P., Langer, N., Podsiadlowski, P., Tauris, T. M. & Moriya, T. J. A new route towards merging massive black holes. *Astron. Astrophys.* **588,** A50 (2016).
13. de Mink, S. E. & Mandel, I. The chemically homogeneous evolutionary channel for binary black hole mergers: rates and properties of gravitational-wave events detectable by advanced LIGO. *Mon. Not. R. Astron. Soc.* http://dx.doi.org/10.1093/mnras/stw1219 (2016).
14. Eldridge, J. J. & Stanway, E. R. BPASS predictions for Binary Black-Hole Mergers. Preprint at http://arxiv.org/abs/1602.03790 (2016).
15. Woosley, S. E. The progenitor of GW150914. Preprint at http://arXiv.org/abs/1603.00511 (2016).
16. Belczynski, K., Kalogera, V. & Bulik, T. A comprehensive study of binary compact objects as gravitational wave sources: evolutionary channels, rates, and physical properties. *Astrophys. J.* **572,** 407–431 (2002).
17. Belczynski, K. *et al.* Compact object modeling with the StarTrack population synthesis code. *Astrophys. J. Suppl. Ser.* **174,** 223–260 (2008).
18. Fryer, C. L. *et al.* Compact remnant mass function: dependence on the explosion mechanism and metallicity. *Astrophys. J.* **749,** 91 (2012).
19. Bulik, T., Belczynski, K. & Prestwich, A. IC10 X-1/NGC300 X-1: the very immediate progenitors of BH-BH binaries. *Astrophys. J.* **730,** 140 (2011).
20. Hirschauer, A. S. *et al.* ALFALFA discovery of the most metal-poor gas-rich galaxy known: AGC 198691. *Astrophys. J.* **822,** 108 (2016).
21. Bulik, T., Gondek-Rosinska, D. & Belczynski, K. Expected masses of merging compact object binaries observed in gravitational waves. *Mon. Not. R. Astron. Soc.* **352,** 1372–1380 (2004).
22. Abbott, B. P. *et al.* The rate of binary black hole mergers inferred from advanced LIGO observations surrounding GW150914. Preprint at http://arxiv.org/abs/1602.03842 (2016).
23. Pavlovskii, K. & Ivanova, N. Mass transfer from giant donors. *Mon. Not. R. Astron. Soc.* **449,** 4415–4427 (2015).
24. Eldridge, J. J., Fraser, M., Smartt, S. J., Maund, J. R. & Crockett, R. M. The death of massive stars – II. Observational constraints on the progenitors of Type Ibc supernovae. *Mon. Not. R. Astron. Soc.* **436,** 774–795 (2013).
25. Gerke, J. R., Kochanek, C. S. & Stanek, K. Z. The search for failed supernovae with the Large Binocular Telescope: first candidates. *Mon. Not. R. Astron. Soc.* **450,** 3289–3305 (2015).
26. Ricker, P. M. & Taam, R. E. The interaction of stellar objects within a common envelope. *Astrophys. J.* **672,** L41–L44 (2008).
27. MacLeod, M. & Ramirez-Ruiz, E. Asymmetric accretion flows within a common envelope. *Astrophys. J.* **803,** 41 (2015).
28. Rogers, T. M., Lin, D. N. C., McElwaine, J. N. & Lau, H. H. B. Internal gravity waves in massive stars: angular momentum transport. *Astrophys. J.* **772,** 21 (2013).
29. Albrecht, S. *et al.* The BANANA project. V. Misaligned and precessing stellar rotation axes in CV Velorum. *Astrophys. J.* **785,** 83 (2014).

Acknowledgements We are indebted to G. Wiktorowicz, W. Gladysz and K. Piszczek for their help with population synthesis calculations, and to H.-Y. Chen and Z. Doctor for their help with our LIGO/Virgo rate calculations. We thank the thousands of Universe@home users that have provided their personal computers for our simulations. We also thank the Hannover GW group for letting us use their ATLAS supercomputer. K.B. acknowledges support from the NCN grant Sonata Bis 2 (DEC-2012/07/E/ST9/01360). D.E.H. was supported by NSF CAREER grant PHY-1151836. D.E.H. also acknowledges support from the Kavli Institute for Cosmological Physics at the University of Chicago through NSF grant PHY-1125897 as well as an endowment from the Kavli Foundation. T.B. acknowledges support from the NCN grant Harmonia 6 (UMO-2014/14/M/ST9/00707). R.O'S. was supported by NSF grant PHY-1505629.

Author Contributions All authors contributed to the analysis and writing of the paper.

Author Information Reprints and permissions information is available at www.nature.com/reprints. The authors declare no competing financial interests. Readers are welcome to comment on the online version of the paper. Correspondence and requests for materials should be addressed to K.B. (chrisbelczynski@gmail.com).

Reviewer Information *Nature* thanks M. Cantiello and the other anonymous reviewer(s) for their contribution to the peer review of this work.

© 2016 Macmillan Publishers Limited. All rights reserved

METHODS

Our Monte Carlo evolutionary modelling is performed with the StarTrack binary population synthesis code[16]. In particular, we incorporate a calibrated treatment of tidal interactions in close binaries[17], a physical measure of the common envelope (CE) binding energy[30,31], and a rapid-explosion supernova model that reproduces the observed mass gap between neutron stars and black holes (BHs)[18,32]. Our updated mass spectrum of BHs shows a strong dependence on the metallicity of the progenitor stars (Extended Data Fig. 5). In galaxies with metallicities similar to the Milky Way ($Z=Z_{\odot}=0.02$), BHs that formed out of single massive stars (initial mass $M_{\rm ZAMS}=150M_{\odot}$) reach a maximum mass of $M_{\rm BH}=15M_{\odot}$, whereas, for very low metallicity ($Z=0.0001=0.005Z_{\odot}$), the maximum mass becomes $M_{\rm BH}=94M_{\odot}$. The above input physics represents our standard model (M1), which is representative of our classical formation scheme for double compact objects (BH–BH, BH–NS and NS–NS).

We have adopted specific values for a number of evolutionary parameters. Single stars are evolved with calibrated formulae based on detailed evolutionary calculations[33]. Massive star winds are adopted from detailed studies of radiation-driven mass loss[34]. For the Luminous Blue Variable phase, a high rate of mass loss is adopted ($1.5\times10^{-4}M_{\odot}\,{\rm yr}^{-1}$). Binary interactions and, in particular, the stability of Roche-lobe overflow (RLOF) is judged on the basis of binary parameters: mass ratio, evolutionary stage of donor, response to mass loss, and behaviour of the orbital separation in response to mass transfer. The orbital separation is additionally affected by gravitational radiation, magnetic braking, and loss of angular momentum associated with systemic mass loss. During stable RLOF, we assume that half of the mass is accreted onto the companion, while the other half ($1-f_{\rm a}=0.5$) is lost with specific angular momentum ($\mathrm{d}J/\mathrm{d}t=j_{\rm loss}[J_{\rm orb}/(M_{\rm don}+M_{\rm acc})](1-f_{\rm a})\mathrm{d}M_{\rm RLOF}/\mathrm{d}t$ with scaling factor $j_{\rm loss}=1.0$ where $f_{\rm a}$ is the fraction of the mass accreted, $J_{\rm orb}$ is the orbital angular momentum, $M_{\rm don}$ is the donor mass, $M_{\rm acc}$ is the accretor mass, and $\mathrm{d}M_{\rm RLOF}/\mathrm{d}t$ is the mass transfer rate; ref. 35). The CE is treated by considering the energy balance with fully effective conversion of orbital energy into envelope ejection (conversion efficiency $\alpha=1.0$), whereas the envelope binding energy for massive stars is calibrated by a parameter λ, which depends on star radius, mass and metallicity. For massive stars, $\lambda\approx0.1$ is adopted[31]. During CE evolution, compact objects accrete at 10% of the Bondi–Hoyle rate as estimated by recent hydrodynamical simulations[26,27]. Our CE evolution is instantaneous, so the time at the beginning and end of the CE phase is exactly the same (see Fig. 1); the time duration of the CE phase has no impact on our results.

We consider two extra variations of the input physics of binary evolution. In one model (M2), we test highly uncertain CE physics[36] and we allow for Hertzsprung-gap stars to initiate and survive CE evolution. This is an optimistic assumption, because these stars may not allow for CE evolution[23], nor survive as a binary if a CE forms[9]. For comparison, in our standard model, we allow only evolved stars with a deep convective envelope (core-helium-burning stars) to survive a CE phase.

In the opposite extreme, we use a model (M3) in which BHs receive large natal kicks. In particular, each BH gets a natal kick with its components drawn from a Maxwellian distribution with a one-dimensional root-mean-square $\sigma=265\,{\rm km\,s^{-1}}$, independent of BH mass. Such large natal kicks are measured for Galactic pulsars[37]. This is a pessimistic assumption, because large natal kicks tend to disrupt BH–BH progenitor binaries. This assumption is not yet excluded on the basis of electromagnetic observations[4]. By contrast, in our standard model, BH natal kicks decrease with BH mass. In particular, for massive BHs that form through direct collapse of an entire star to a BH with no supernova explosion ($M_{\rm BH}\gtrsim10M_{\odot}$ for $Z=Z_{\odot}$, $M_{\rm BH}\gtrsim15M_{\odot}$ for $Z=0.1Z_{\odot}$ and $M_{\rm BH}\gtrsim15M_{\odot}$–$30M_{\odot}$ for $Z=0.01Z_{\odot}$), we assume no natal kicks[18]. We also calculated a series of models with intermediate BH kicks (see Extended Data Fig. 4): $\sigma=200\,{\rm km\,s^{-1}}$ (model M4), $\sigma=130\,{\rm km\,s^{-1}}$ (model M5) and $\sigma=70\,{\rm km\,s^{-1}}$ (model M6).

For each evolutionary model we compute 2×10^{7} massive binaries for each point on a grid of 32 sub-models covering a wide range of metallicities: $Z=0.0001$, 0.0002, 0.0003, 0.0004, 0.0005, 0.0006, 0.0007, 0.0008, 0.0009, 0.001, 0.0015, 0.002, 0.0025, 0.003, 0.0035, 0.004, 0.0045, 0.005, 0.0055, 0.006, 0.0065, 0.007, 0.0075, 0.008, 0.0085, 0.009, 0.0095, 0.01, 0.015, 0.02, 0.025 and 0.03. We assume that stellar evolution at even lower metallicities proceeds in the same way as the evolution at $Z=0.005Z_{\odot}$. However, stars with very low metal content (for example, Population III) may evolve differently to metal-rich stars[38].

Each sub-model is computed with initial distributions of orbital periods P (proportional to $[\log(P)]^{-0.5}$), eccentricities e (proportional to $e^{-0.42}$) and mass ratios q (proportional to q^{0}) appropriate for massive stars[39]. We adopt an initial mass function that is close to flat for low-mass stars (proportional to $M^{-1.3}$ for $0.08M_{\odot}\leq M<0.5M_{\odot}$ and to $M^{-2.2}$ for $0.5M_{\odot}\leq M<1.0M_{\odot}$) and that is top-heavy for massive stars (proportional to $M^{-2.3}$ for $1.0M_{\odot}\leq M\leq150M_{\odot}$), as guided by recent observations[40]. The adopted initial mass function generates higher BH–BH merger-rate densities as compared with the steeper initial mass function (proportional to $M^{-2.7}$ for $1.0M_{\odot}\leq M\leq150M_{\odot}$) adopted in previous studies[4,41], because there are more BH–BH merger progenitors in our simulations[42].

A moderate binary fraction ($f_{\rm bi}=0.5$) is adopted for stars with masses $M_{\rm ZAMS}<10M_{\odot}$, whereas we assume that all more massive stars are formed in binaries ($f_{\rm bi}=1.0$), as indicated by recent empirical estimates[39,43].

We adopt an extinction-corrected cosmic star-formation rate (SFR) based on numerous multi-wavelength observations[44]:

$$\mathrm{SFR}\,(z)=0.015\frac{(1+z)^{2.7}}{1+[(1+z)/2.9]^{5.6}}M_{\odot}\,{\rm Mpc^{-3}\,yr^{-1}} \qquad (1)$$

This SFR declines rapidly at high redshifts ($z>2$). This may be contrasted with some SFR models used previously[45], which generated a greater number of stars at high redshifts. This revision will thus reduce the BH–BH merger-rate densities at all redshifts. Even though the formation of BH–BH binaries takes a very short time (about 5 Myr), the time to coalescence of two BHs may be very large (Fig. 1 and Extended Data Fig. 2).

In our treatment of chemical enrichment of the Universe, we follow the mean metallicity increase with cosmic time (since Big Bang until present). The mean metallicity as a function of redshift is:

$$\log[Z_{\rm mean}(z)]=0.5+\log\left(\frac{y\,(1-R)}{\rho_{\rm b}}\int_{z}^{20}\frac{97.8\times10^{10}\mathrm{SFR}(z')}{H_0E(z')(1+z')}\mathrm{d}z'\right)$$

with a return fraction $R=0.27$ (mass fraction of each generation of stars that is put back into the interstellar medium), a net metal yield $y=0.019$ (mass of new metal created and ejected into the interstellar medium by each generation of stars per unit mass locked in stars), a baryon density $\rho_{\rm b}=2.77\times10^{11}\,\Omega_{\rm b}\,h_0^2M_{\odot}\,{\rm Mpc^{-3}}$ with $\Omega_{\rm b}=0.045$ and $h_0=0.7$, a SFR given by Equation (1), and $E(z)=\sqrt{\Omega_{\rm M}(1+z)^3+\Omega_{\rm k}(1+z)^2+\Omega_{\Lambda}}$ with $\Omega_{\Lambda}=0.7$, $\Omega_{\rm M}=0.3$, $\Omega_{\rm k}=0$ and $H_0=70.0\,{\rm km\,s^{-1}\,Mpc^{-1}}$. The shape of the mean-metallicity dependence on redshift follows recent estimates[44], although the level was increased by 0.5 dex to better fit observational data[46]. At each redshift, we assume a log-normal distribution of metallicity around the mean, with a standard deviation of $\sigma=0.5$ dex (ref. 47). Our prescription (Extended Data Fig. 6) produces more low-metallicity stars than previously[41]. Because BH–BH formation is enhanced at low-metallicity[2], our new approach increases the predicted rate densities of BH–BH mergers.

Here we discuss caveats of evolutionary calculations. First, we consider only isolated binary evolution, and thus our approach is applicable to field stars in low-density environments. It is possible that dynamical interactions enhance BH–BH merger formation in dense globular clusters[11], offering a completely independent channel.

Second, our predictions are based on a 'classical' theory of stellar and binary evolution for the modelling of massive stars that we have compiled, developed and calibrated over the last 15 years. We do not consider exotic channels for the formation of BH–BH mergers, such as the one from rapidly rotating stars in contact binaries[48].

Third, our modelling includes only three evolutionary models: a standard model consisting of our best estimates for reasonable parameters (M1), as well as optimistic (M2) and pessimistic (M3) alternative models. The optimistic model consists of only one change from the standard model: we allow all stars beyond the main sequence to survive the CE phase. Alternatively, the pessimistic model also consists of only one change: larger BH natal kicks. We have not investigated other possible deviations from the standard model (for example, different assumptions of mass and angular-momentum loss during stable mass-transfer evolution) nor have we checked inter-parameter degeneracies (for example, models with large BH kicks and an optimistic CE phase). Precursor versions of these computationally demanding studies have already been performed[49], albeit with low statistics and limited scope; these calculations indicate that our three models probably cover the range of interesting effects.

Fourth, our observations are severely statistically limited. We are attempting to draw inferences about our models on the basis of a single detection (GW150914).

In was argued[50] that the formation of GW150914 in isolated binary evolution requires a metallicity lower than $0.5Z_{\odot}$. This argument was based on single stellar models[51]; stars in close binaries are subject to significant mass loss during RLOF/CE, and they form BHs with lower mass than BHs formed by single stars. Thus, in binaries, the metallicity threshold for massive BH formation is lower than in single stellar evolution. For example, formation of a single $30M_{\odot}$ BH requires $Z<0.25Z_{\odot}$ (Extended Data Fig. 5, whereas formation of two such BHs in a binary requires $Z<0.10Z_{\odot}$ (Extended Data Fig. 1). The value of this threshold depends on assumptions for the model of stellar evolution, winds and BH formation

© 2016 Macmillan Publishers Limited. All rights reserved

processes. The physical models we have adopted yield a threshold of $Z < 0.10Z_{\odot}$, the same as that obtained with MESA (http://mesa.sourceforge.net/) for homogeneous stellar evolution[12]. Our model was calibrated using known masses of BHs and, in particular, we do not exceed $15M_{\odot}$ for $Z_{\odot}$ (the highest-mass stellar BH known in our Galaxy). By contrast, single stellar models used to derive the high metallicity threshold produce $25M_{\odot}$ for $Z_{\odot}$ (ref. 51). The highest threshold obtained with binary evolution was reported at the level of $0.5Z_{\odot}$ (ref. 14). Such a high value of the metallicity threshold for the progenitor of GW150914 implies that stars at approximately solar metallicity ($Z = 0.014$) produce BHs as massive as $40M_{\odot}$ (ref. 14). This is neither supported nor excluded by available electromagnetic BH mass measurements (https://stellarcollapse.org/bhmasses).

In the following, we present calculation of the gravitational radiation signal. The output of StarTrack is a binary merger at a given time. We then calculate the gravitational waveform associated with this merger, and determine whether this binary would have been observable by LIGO in the O1 configuration[3,4].

We model the full inspiral–merger–ringdown waveform of the binaries using the IMRPhenomD gravitational waveform template family[52,53]. This is a simple and fast waveform family that neglects the effects of spin (which are not relevant for GW150914). We consider a detection to be given by a threshold of SNR > 8 in a single detector, and we use the fiducial O1 noise curve (https://dcc.ligo.org/LIGO-G1501223/public). We calculate the face-on, overhead SNR for each binary directly from equation (2) of ref. 3. We then calculate the luminosity distance at which this binary would be detected with SNR = 8. As the distance to the binary changes, the observer-frame (redshifted) mass also changes, and therefore calculating the horizon redshift requires an iterative process. Once this has been calculated, we then determine the predicted detection rates using equation (9) of ref. 3; the effects of the antenna power pattern are incorporated in the p_{det} term in this equation.

An estimate of fiducial advanced LIGO sensitivity during the 16-day GW150914 analysis is shown in Fig. 3. We estimate the sensitivity to coalescing compact binaries using a reference O1 noise curve. We assume that both detectors operate with the fiducial O1 noise curve, which is the same sensitivity we adopted to calculate compact binary detection rates. For comparison, this model agrees reasonably well with the 'early-high' sensitivity model[54]. Our expression is a 50th percentile upper limit, assuming no detections. The critical application of this expression is not related to its overall normalization; we are instead interested in its shape, which characterizes the strongly mass-dependent selection biases of LIGO searches.

Using these inputs, our fiducial estimate of the advanced LIGO sensitivity during the first 16 days of O1 for a specific mass bin ΔM_i is:

$$R_{\mathrm{D},\Delta M_i,\mathrm{UL}} = \frac{0.7}{V_{\Delta M_i} T}$$

where $T = 16$ days corresponds to the analysis of GW150914[1], the volume:

$$V_{\Delta M_i} = \frac{1}{\Delta M_i} \int \mathrm{d}M \int \frac{\mathrm{d}z}{1+z} \frac{\mathrm{d}V}{\mathrm{d}z} p_{\mathrm{det}}(w, M)$$

is the sensitive volume averaged over mass bin ΔM_i, and $p_{\mathrm{det}}(w, M)$ is the orientation-averaged detection probability[3,4]. The function $p_{\mathrm{det}}(w, M)$ depends on the coalescing binary redshifted mass M through the maximum luminosity distance ('horizon distance') at which a source could produce a response of SNR >8 in a single detector through a projection parameter w, which is maximum ($w = 1$) for a face-on, overhead source, and minimum ($w = 0$) for sky locations and orientations where the LIGO detector has no response to the source. To calculate this distance, we adopt the IMRPhenomD gravitational waveforms[52,53] that we also used to estimate compact binary detection rates. Extended Data Fig. 7 shows our estimated horizon redshift as a function of the total redshifted binary merger mass for equal-mass mergers.

Code availability. We have opted not to release the population synthesis code StarTrack used to generate binary populations for this study.

30. Dominik, M. *et al.* Double compact objects. I. The significance of the common envelope on merger rates. *Astrophys. J.* **759,** 52 (2012).
31. Xu, X.-J. & Li, X.-D. Erratum: "On the binding energy parameter λ of common envelope evolution" (2010, ApJ, 716, 114). *Astrophys. J.* **722,** 1985–1988 (2010).
32. Belczynski, K., Wiktorowicz, G., Fryer, C. L., Holz, D. E. & Kalogera, V. Missing black holes unveil the supernova explosion mechanism. *Astrophys. J.* **757,** 91 (2012).
33. Hurley, J. R., Pols, O. R. & Tout, C. A. Comprehensive analytic formulae for stellar evolution as a function of mass and metallicity. *Mon. Not. R. Astron. Soc.* **315,** 543–569 (2000).
34. Vink, J. S. The theory of stellar winds. *Astrophys. Space Sci.* **336,** 163–167 (2011).
35. Podsiadlowski, P., Joss, P. C. & Hsu, J. J. L. Presupernova evolution in massive interacting binaries. *Astrophys. J.* **391,** 246–264 (1992).
36. Ivanova, N. *et al.* Common envelope evolution: where we stand and how we can move forward. *Astron. Astrophys. Rev.* **21,** 59 (2013).
37. Hobbs, G., Lorimer, D. R., Lyne, A. G. & Kramer, M. A statistical study of 233 pulsar proper motions. *Mon. Not. R. Astron. Soc.* **360,** 974–992 (2005).
38. Szécsi, D. *et al.* Low-metallicity massive single stars with rotation. Evolutionary models applicable to I Zwicky 18. *Astron. Astrophys.* **581,** A15 (2015).
39. Sana, H. *et al.* Binary interaction dominates the evolution of massive stars. *Science* **337,** 444–446 (2012).
40. Bastian, N., Covey, K. R. & Meyer, M. R. A universal stellar initial mass function? A critical look at variations. *Annu. Rev. Astron. Astrophys.* **48,** 339–389 (2010).
41. Dominik, M. *et al.* Double compact objects. II. Cosmological merger rates. *Astrophys. J.* **779,** 72 (2013).
42. de Mink, S. E. & Belczynski, K. Merger rates of double neutron stars and stellar origin black holes: the impact of initial conditions on binary evolution predictions. *Astrophys. J.* **814,** 58 (2015).
43. Duchêne, G. & Kraus, A. Stellar multiplicity. *Annu. Rev. Astron. Astrophys.* **51,** 269–310 (2013).
44. Madau, P. & Dickinson, M. Cosmic star-formation history. *Annu. Rev. Astron. Astrophys.* **52,** 415–486 (2014).
45. Strolger, L.-G. *et al.* The *Hubble* Higher *z* Supernova Search: supernovae to $z \approx 1.6$ and constraints on Type Ia progenitor models. *Astrophys. J.* **613,** 200–223 (2004).
46. Vangioni, E. *et al.* The impact of star formation and gamma-ray burst rates at high redshift on cosmic chemical evolution and reionization. *Mon. Not. R. Astron. Soc.* **447,** 2575–2587 (2015).
47. Dvorkin, I., Silk, J., Vangioni, E., Petitjean, P. & Olive, K. A. The origin of dispersion in DLA metallicities. *Mon. Not. R. Astron. Soc.* **452,** L36–L40 (2015).
48. Almeida, L. A. *et al.* Discovery of the massive overcontact binary VFTS 352: evidence for enhanced internal mixing. *Astrophys. J.* **812,** 102 (2015).
49. O'Shaughnessy, R., Kalogera, V. & Belczynski, K. Mapping population synthesis event rates on model parameters. II. Convergence and accuracy of multidimensional fits. *Astrophys. J.* **667,** 1048–1058 (2007).
50. Abbott, B. P. *et al.* Astrophysical implications of the binary black hole merger GW150914. *Astrophys. J.* **818,** L22 (2016).
51. Spera, M., Mapelli, M. & Bressan, A. The mass spectrum of compact remnants from the PARSEC stellar evolution tracks. *Mon. Not. R. Astron. Soc.* **451,** 4086–4103 (2015).
52. Khan, S. *et al.* Frequency-domain gravitational waves from nonprecessing black-hole binaries. II. A phenomenological model for the advanced detector era. *Phys. Rev. D* **93,** 044007 (2016).
53. Husa, S. *et al.* Frequency-domain gravitational waves from nonprecessing black-hole binaries. I. New numerical waveforms and anatomy of the signal. *Phys. Rev. D* **93,** 044006 (2016).
54. Abbott, B. P. *et al.* Prospects for observing and localizing gravitational-wave transients with Advanced LIGO and Advanced Virgo. *Living Rev. Relativ.* **19,** 1 (2013).
55. Villante, F. L., Serenelli, A. M., Delahaye, F. & Pinsonneault, M. H. The chemical composition of the sun from helioseismic and solar neutrino data. *Astrophys. J.* **787,** 13 (2014).

© 2016 Macmillan Publishers Limited. All rights reserved

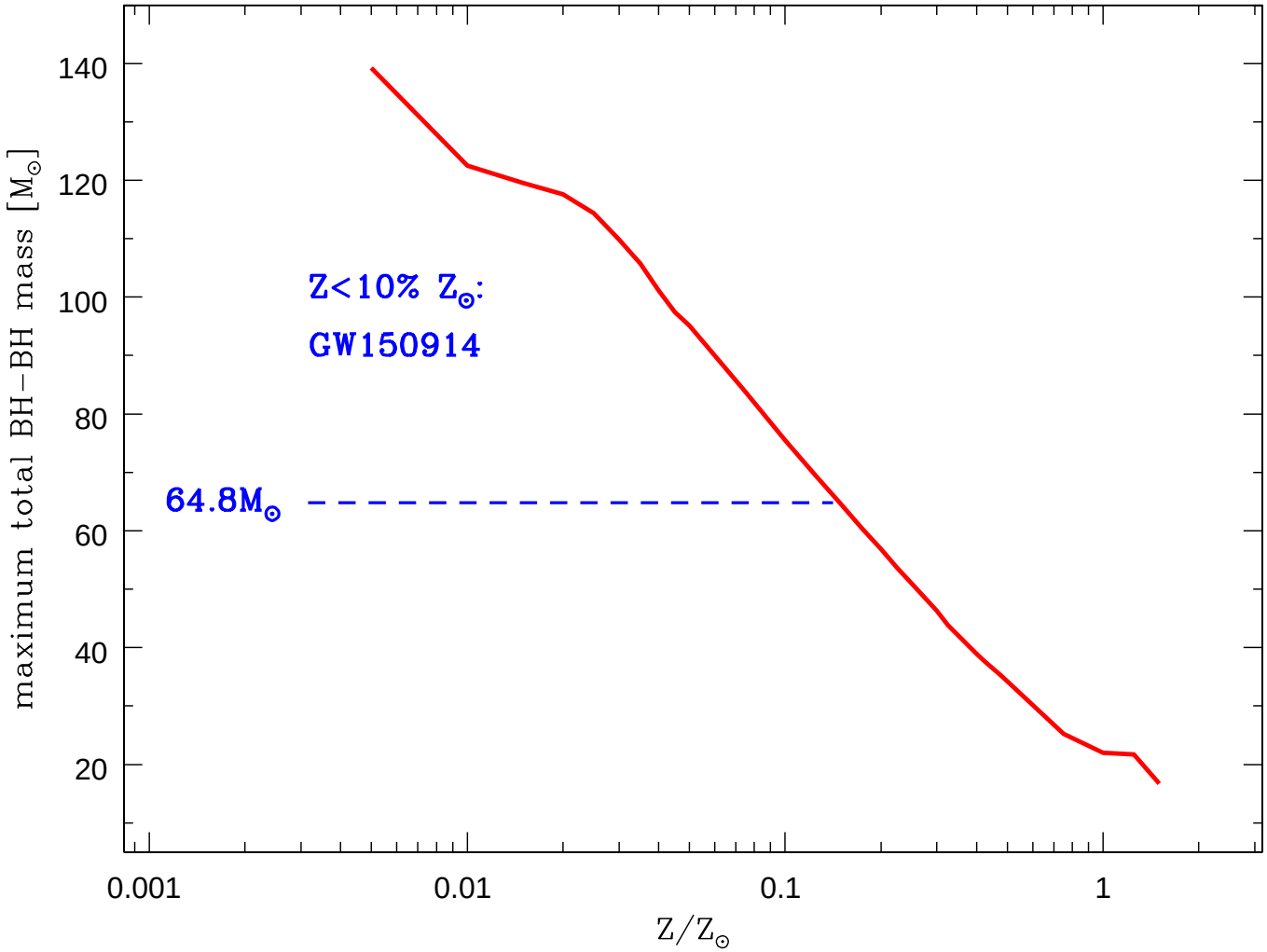

Extended Data Figure 1 | Maximum total mass of BH–BH mergers as a function of metallicity. Binary stars at metallicities $Z < 0.1Z_{\odot}$ can form BH–BH mergers that are more massive than $M_{\rm tot} = 64.8M_{\odot}$. This suggests that GW150914 was formed in a low-metallicity environment, assuming it is a product of classical isolated binary evolution. The total binary-maximum BH–BH mass is not a simple sum of maximum BH masses resulting from single stellar evolution; this is a result of mass loss during the RLOF and CE evolution phases in the formation of massive BH–BH mergers (Fig. 1).

© 2016 Macmillan Publishers Limited. All rights reserved

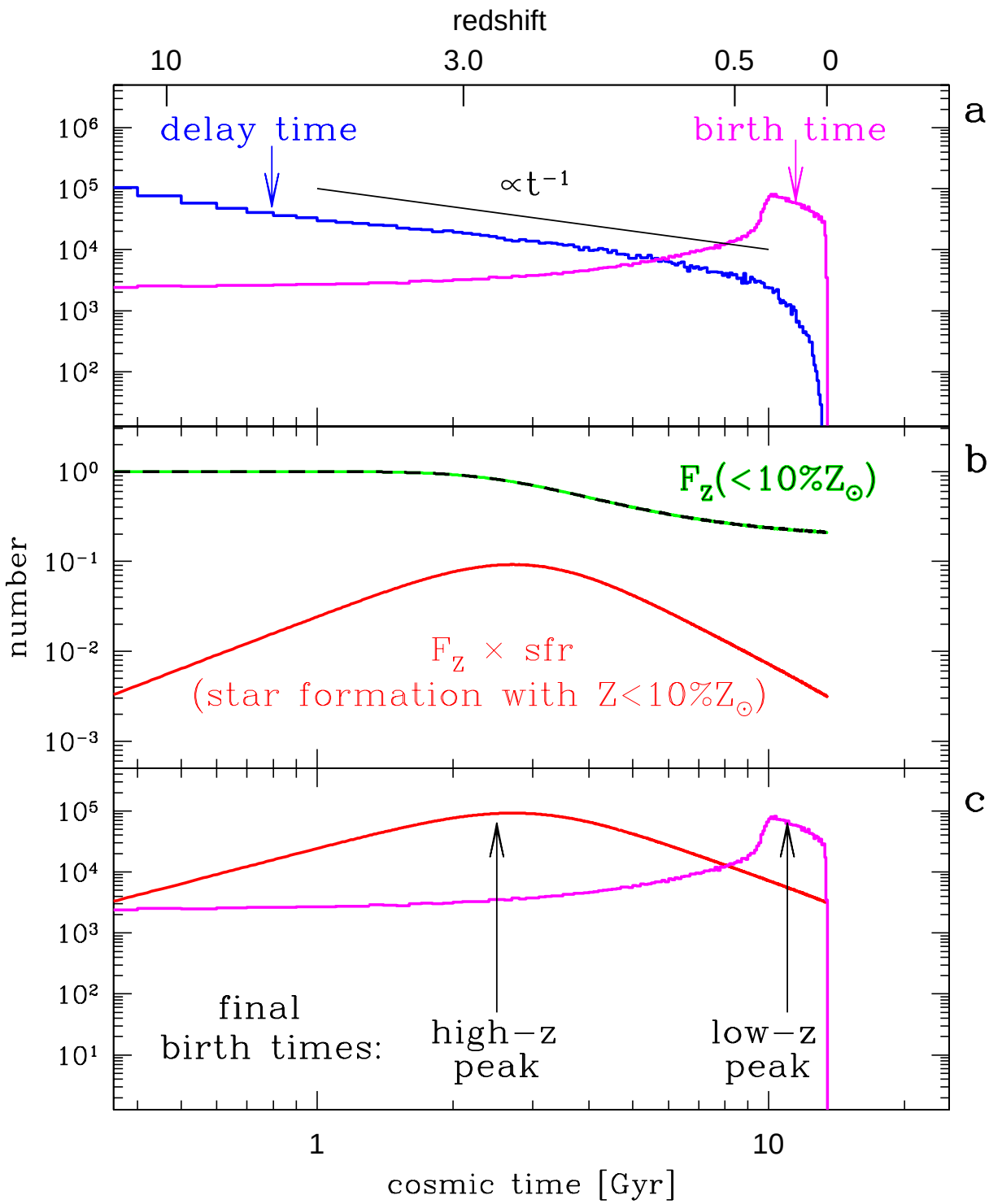

Extended Data Figure 2 | Emergence of a bimodal birth-time distribution. a, BH binaries follow an intrinsic power-law delay-time distribution (proportional to t^{-1}). The birth time ($t_{\mathrm{birth}} = t_{\mathrm{merger}} - t_{\mathrm{delay}}$) is inverted compared to the delay-time distribution (blue line), with the spread caused by allowing the merger time (t_{merger}) to fall anywhere within the O1 LIGO horizon: $z = 0$–0.7; this generates a peak corresponding to BH–BH progenitors born late with short delay times. **b**, Massive BH–BH binaries are formed by only low-metallicity stars ($Z < 0.10 Z_{\odot}$). The fraction of all stars that form at such low Z (F_Z) decreases with cosmic time, making low-Z star formation (in units of $M_{\odot}\ \mathrm{Mpc}^{-3}\ \mathrm{yr}_{-}1$) peak at early cosmic time. sfr, star-formation rate. **c**, The final birth-time distribution for massive BH–BH mergers is a convolution of the intrinsic birth times and the low-metallicity star-formation rate.

© 2016 Macmillan Publishers Limited. All rights reserved

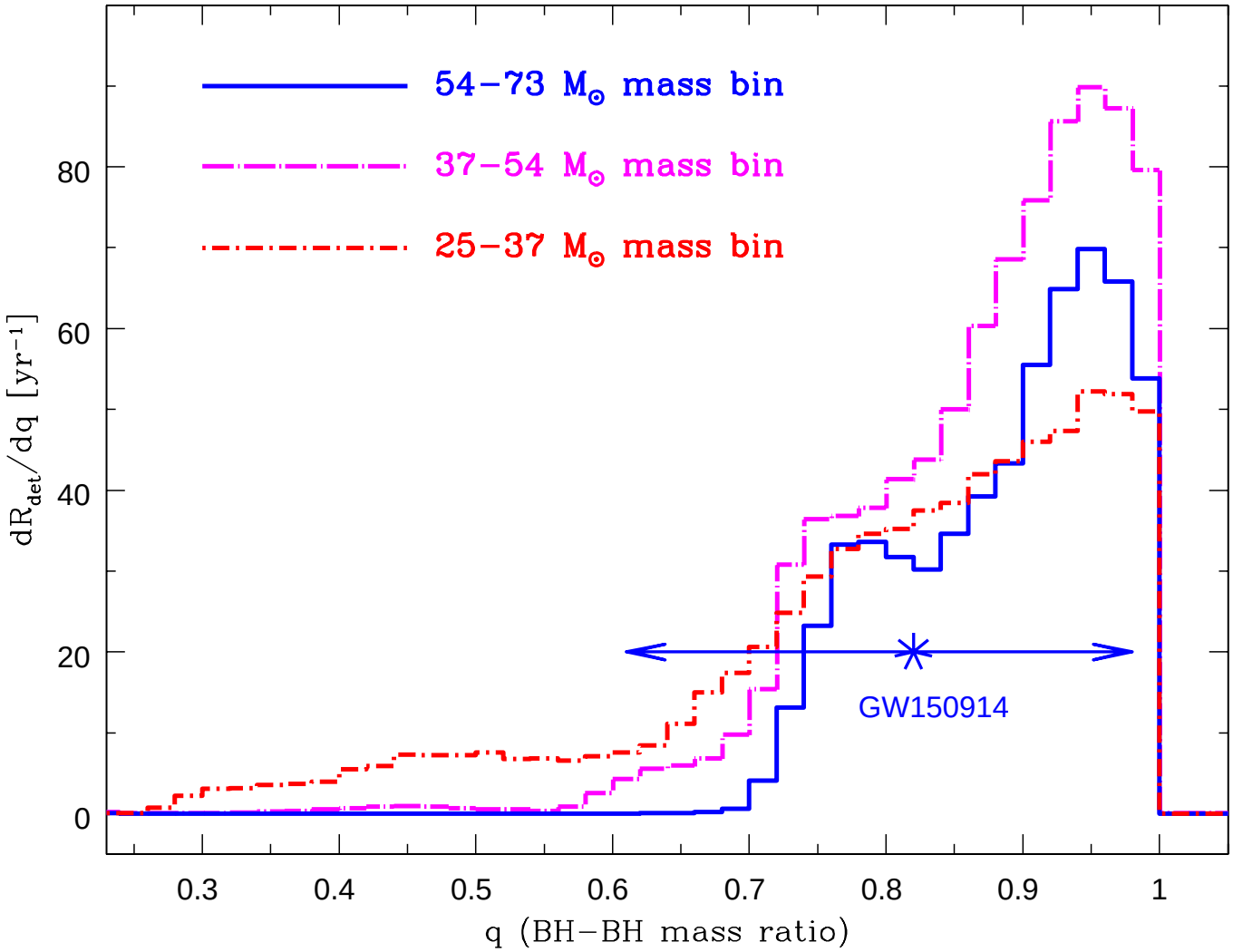

Extended Data Figure 3 | Predicted distribution of BH–BH merger mass ratios. dR_{det}/dq is the contribution to the detection rate, R_{det}, from binaries within a given 0.02 bin in mass ratio, q. Standard model (M1) detector-frame mass ratio is shown. BH–BH binaries prefer mass ratios of $q \gtrsim 0.7$, with a prominent peak near comparable-mass systems. GW150914, with $q = 0.82^{+0.16}_{-0.21}$ (90% credible range) and a total redshifted mass of $M_{tot,z} = 70.5 M_{\odot}$, falls within the expected region.

© 2016 Macmillan Publishers Limited. All rights reserved

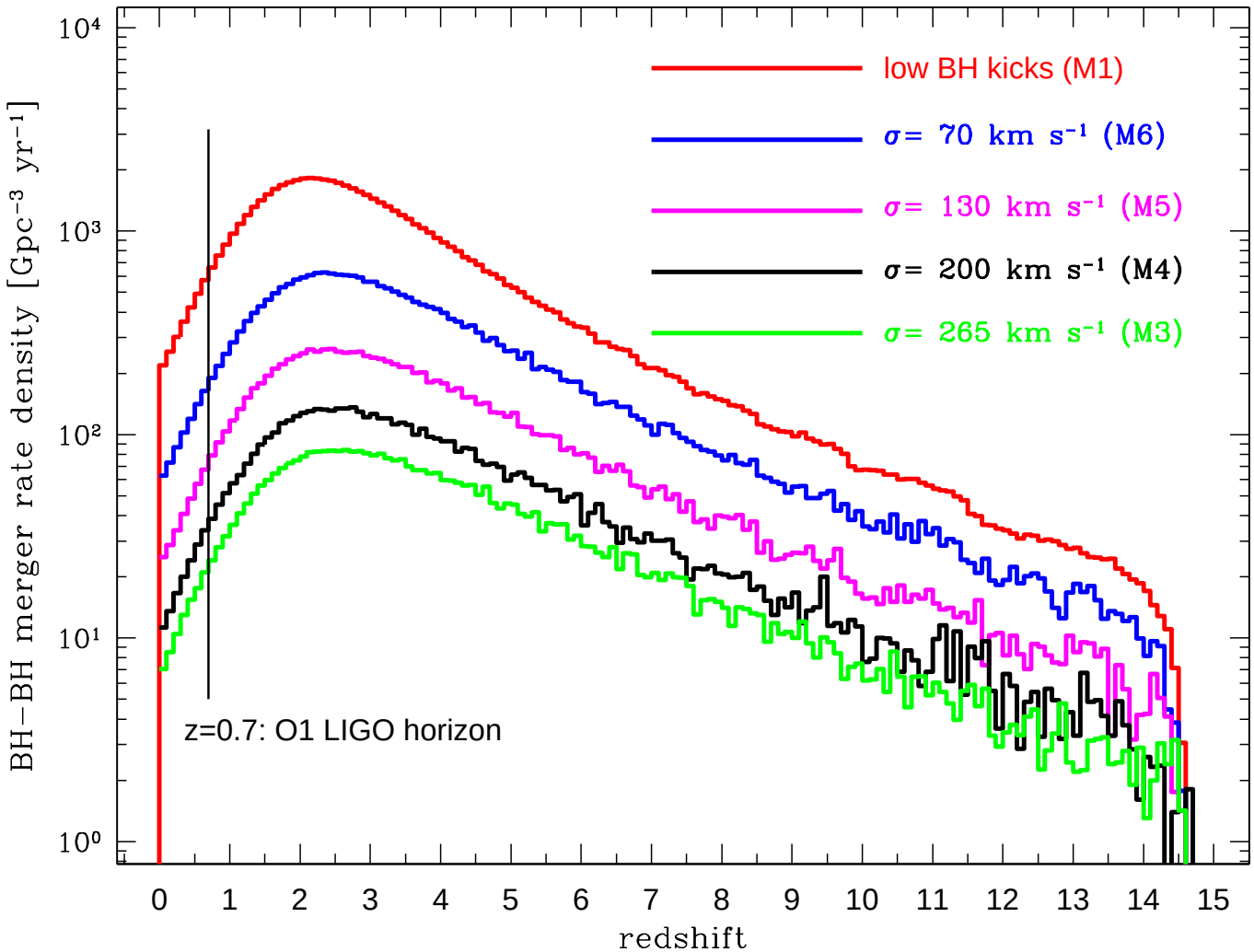

Extended Data Figure 4 | Source-frame merger-rate density for BH–BH binaries as a function of redshift. The red line shows the results from our standard model (M1); in this model, massive BHs do not get natal kicks. A sequence of models with increasing BH natal kicks (models M6, M5, M4, M3) is shown. The rate density decreases with increasing natal kick strength described by a Maxwellian distribution with a one-dimensional root mean square deviation of σ. The local merger-rate density ($z < 0.1$) changes from 218 $\mathrm{Gpc^{-3}\,yr^{-1}}$ (M1) to 63 $\mathrm{Gpc^{-3}\,yr^{-1}}$ (M6), 25 $\mathrm{Gpc^{-3}\,yr^{-1}}$ (M5), 11 $\mathrm{Gpc^{-3}\,yr^{-1}}$ (M4) and 6.6 $\mathrm{Gpc^{-3}\,yr^{-1}}$ (M3). The LIGO estimate (2–400 $\mathrm{Gpc^{-3}\,yr^{-1}}$) encompasses all of these models. We mark the O1 LIGO detection horizon ($z = 0.7$; see Extended Data Fig. 7).

© 2016 Macmillan Publishers Limited. All rights reserved

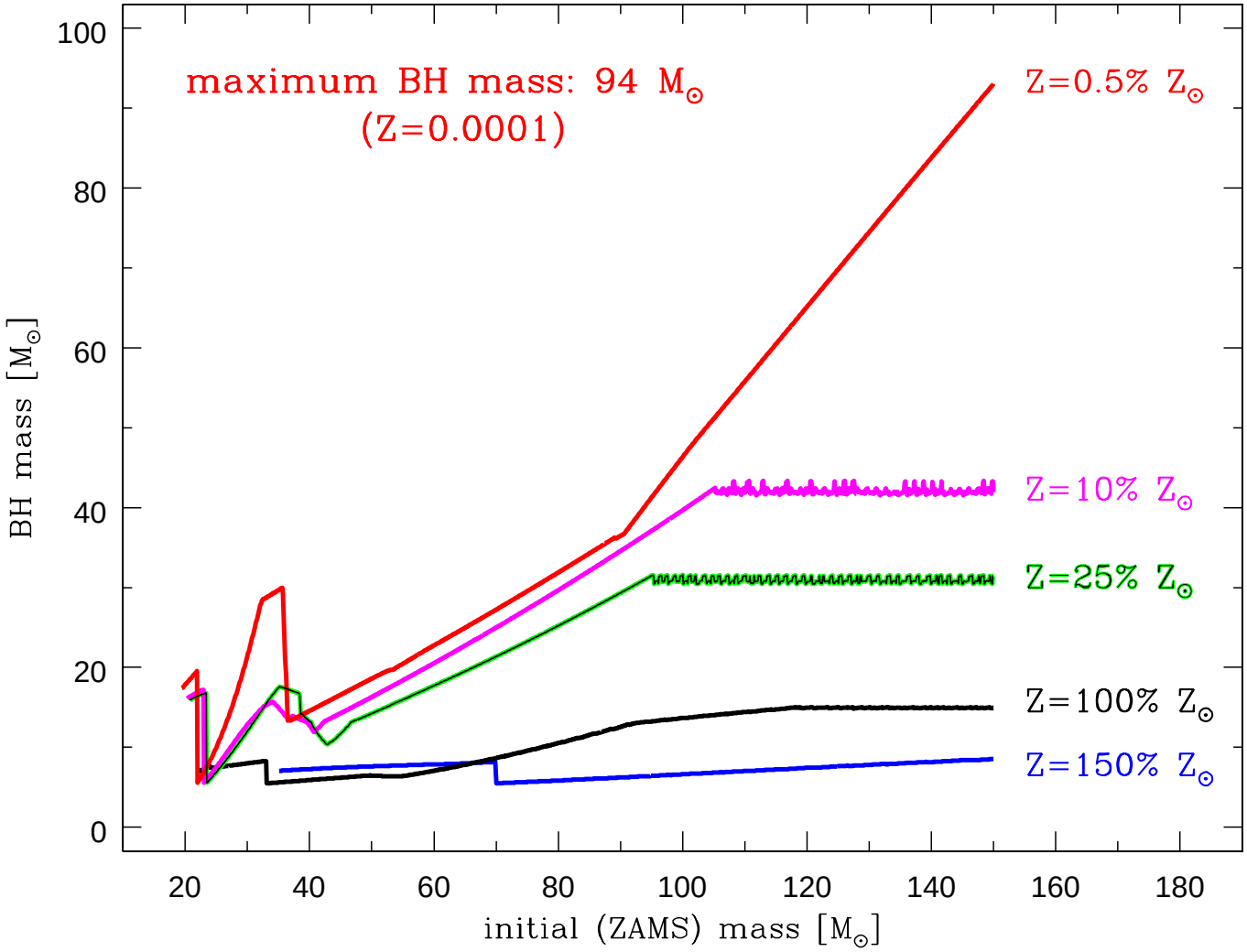

Extended Data Figure 5 | BH mass as a function of initial star mass, for a range of metallicities. These results show calculations for single star evolution with no binary interactions. Our updated models of BH formation show a general increase of BH mass with initial progenitor star mass. There is strong dependence of BH mass on the chemical composition of the progenitor. For example, the maximum BH mass increases from $10M_{\odot}$–$15M_{\odot}$ for high-metallicity progenitors ($Z = 1.5Z_{\odot}$–$1Z_{\odot}$) to $94M_{\odot}$ for low-metallicity progenitors ($Z = 0.005Z_{\odot}$). The formation of a single $30M_{\odot}$ BH requires a metallicity of $Z \leq 0.25Z_{\odot}$. ZAMS, zero-ago main sequence.

© 2016 Macmillan Publishers Limited. All rights reserved

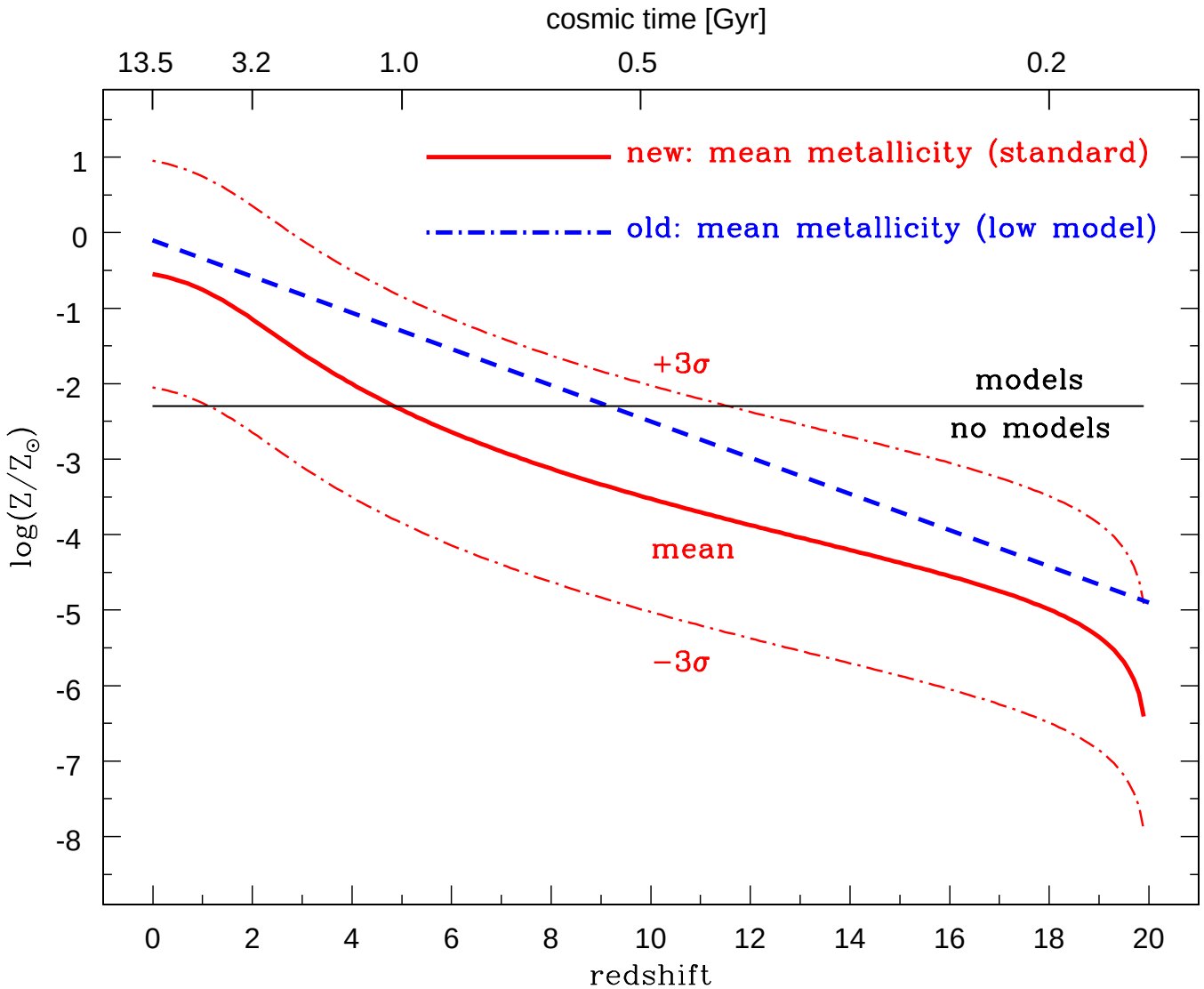

Extended Data Figure 6 | Mean-metallicity evolution of the Universe with redshift. It is assumed that at each redshift the metallicity distribution is log-normal with a standard deviation of $\sigma = 0.5$ dex. The blue line denotes the mean-metallicity evolution adopted in previous studies. The new relation generates more low-metallicity stars at all redshifts. We mark the line above which we can make predictions ($\log(Z/Z_{\odot}) = -2.3$, $Z_{\odot} = 0.02$; ref. 55) based on actual evolutionary stellar models adopted in our calculations. Below this line we assume that stars produce BH–BH mergers in the same way as in the case of our lowest available model.

© 2016 Macmillan Publishers Limited. All rights reserved

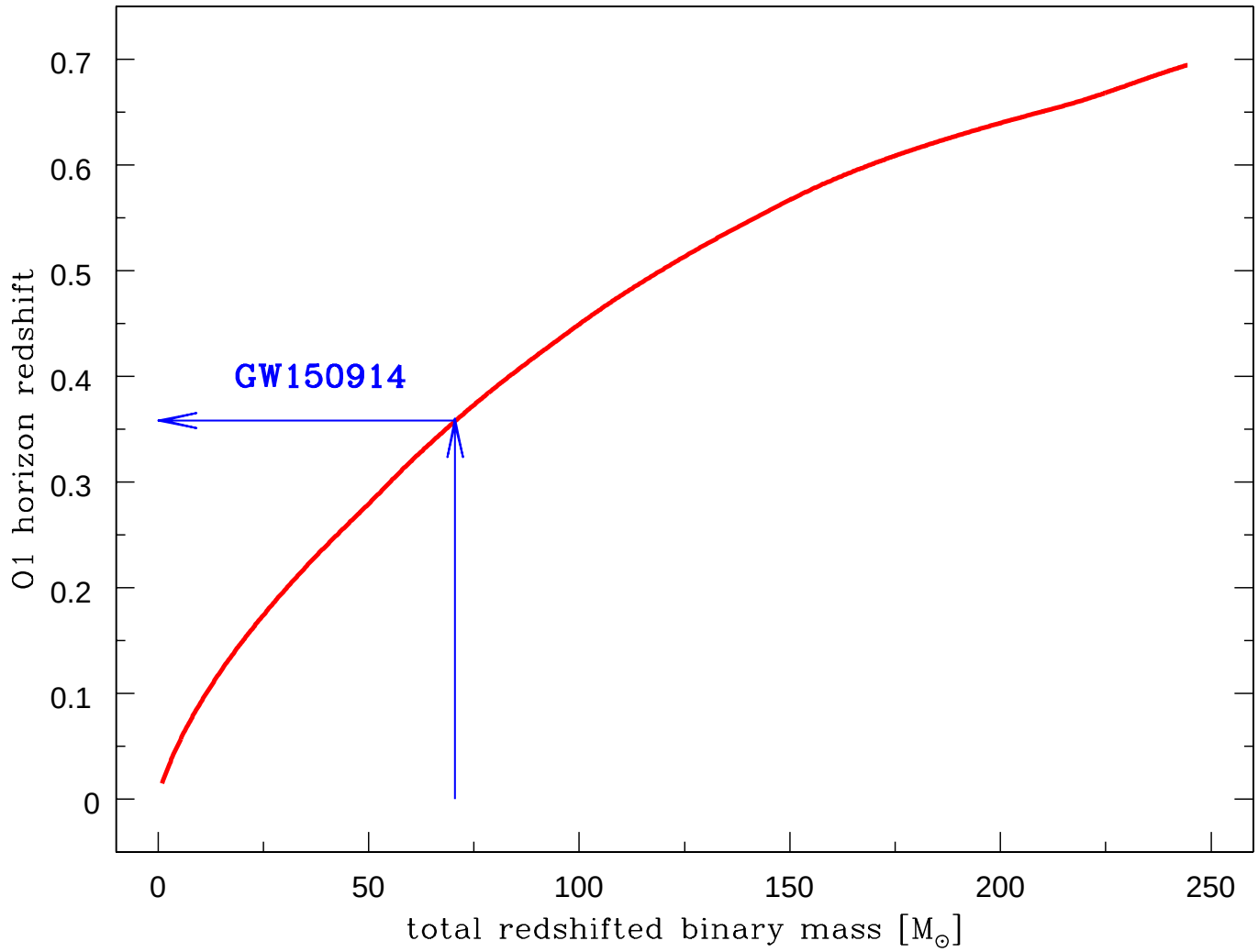

Extended Data Figure 7 | Horizon redshift for the first advanced LIGO observational run (O1). Horizon is given as a function of the total redshifted binary merger mass (assuming equal-mass mergers). For the highest-mass mergers found in our simulations ($M_{\mathrm{tot},z} = 240 M_{\odot}$), the horizon redshift is $z_{\mathrm{hor}} = 0.7$. For GW150914 ($M_{\mathrm{tot},z} = 70.5 M_{\odot}$), the horizon redshift is $z_{\mathrm{hor}} = 0.36$.

© 2016 Macmillan Publishers Limited. All rights reserved

Extended Data Table 1 | Formation channels of massive BH–BH mergers (M1)

Channel	Evolutionary sequence	all [%]	high-z	mid-z	low-z
BHBH1	MT1(2-1) BH1 CE2(14-4;14-7) BH2	79.481	38.045	18.673	22.763
BHBH2	MT1(4-1) BH1 CE2(14-4;14-7) BH2	13.461	10.766	1.101	1.594
BHBH3	MT1(4-4) CE2(4/7-4;7-7) BH1 BH2	5.363	4.852	0.194	0.317
Other	additional combinations	1.696	0.625	0.421	0.649

The first two columns identify evolutionary sequences leading to the formation of BH–BH mergers with $M_{\mathrm{tot},z} = 54M_{\odot}$–$73M_{\odot}$. The third column lists the formation efficiency. The last three columns list the formation efficiency of BH–BH progenitors born at $z > 1.12$, $1.12 < z < 0.34$, $z < 0.34$. Notation: stable mass transfer (MT), common envelope (CE), BH formation (BH) initiated by either the primary star (1) or the secondary star (2). In parentheses we give the evolutionary stage of stars during MT/(pre-;post-)CE: main sequence (1), Hertzsprung gap (2), core helium-burning (4), helium star (7) or BH (14), with the primary star listed first.

© 2016 Macmillan Publishers Limited. All rights reserved